Proc. 8th American Nuclear Society Topical Meeting on Robotics and Remote Systems, Pittsburgh, PA, April 1999.

Monitoring and Diagnostics for a Hydraulic Robot in Hazardous Environments

Martin L. Leuschen
Rice University
ECE Dept.
6100 S. Main, MS 366
Houston, TX 77005
martinl@rice.edu
Tel: (713) 527-8101x2256

Joseph R. Cavallaro
Rice University
ECE Dept.
6100 S. Main, MS 366
Houston, TX 77005
cavallar@rice.edu
Tel: (713) 527-4719

Ian D. Walker
Clemson University
ECE Dept.
Fluor Daniel Building
Clemson, SC 29634
ianw@ces.clemson.edu
Tel: (864) 656-7209

ABSTRACT

Hazardous environments are an important application of modern robotic techniques. However, failures can be quite serious in such environments, especially if they trap the robot within or damage containment efforts. Thus robust early fault detection is especially important for such robots. In this paper we discuss the application of one such method, analytical redundancy, to a hydraulic system similar to the one found in hazardous environment robots such as the Rosie worksystem. Further, we extend the method beyond its linear formulation to better deal with the nonlinearities inherent to hydraulic systems.

1. Introduction

One of the most important and fast growing areas in the robotics industry is the development of robots capable of working in hazardous environments [4, 5, 6, 12]. Providing a high level of functionality in these arenas is important simply because humans cannot safely or cheaply work there. This allows completion of previously impossible tasks and often involves the creation of new jobs rather than the destruction of old ones.

The usefulness of robots in hazardous situations is highly dependent on their reliability. Hazardous environments can damage robotic components, and many of them can be made *more* hazardous by the presence of a malfunctioning robot. Additionally, humans usually cannot enter these areas to repair or remove a failed robot. For these reasons, our team has investigated reliability issues for robots extensively [7, 8, 9].

The Rosie mobile worksystem [1, 3] is an important and interesting example robot that is on the cutting edge of hazardous environment robotics, which has served as our inspiration and motivation for this work. Rosie, under development by RedZone Robotics Inc. and Carnegie Mellon University's Field Robotics Center, is a heavy-duty hydraulic robot designed for nuclear reactor decontamination and dismantlement. The robot has four independently steerable wheels powered by hydraulic motors supporting a chassis sporting a heavy-duty crane/manipulator. Fault detection for Rosie is interesting

and important, and we are additionally using Rosie as a intermediate step to begin looking at fault detection for hydraulic systems in general.

This paper will focus on a method known as *analytical redundancy* [2, 9], or AR. AR is a model-based state-space technique that derives the maximum number of independent tests of the consistency of sensor data with the linearized system model and past control inputs. It yields tests to determine whether the system is performing nominally, or is deviating from the desired plan and presumably under fault conditions. Our group has used this technique successfully on electrical robotic systems in the past [12], and is now applying it to the hydraulic Rosie-like systems.

In a previous paper [9], we discussed the derivation through AR of a suite of model based tests for the default sensor package for hydraulic wheel actuators. Some of these tests are comparison of the actual system response to control inputs to the predicted response indicated by the model. The other tests uncovered by the AR analysis reflect higher order state interdependencies.

However, due to the state-space nature of AR, these tests are all inherently linear. However, the hydraulic valve and motor system behavior is highly nonlinear in nature, which leads to a degradation in the performance of the AR method. In this paper, we will show how to formally extend the linear AR tests into the nonlinear realm, making the AR method suitable for analysis of nonlinear systems such as this.

2. Hydraulic Model and Testbed

The hydraulic wheel actuator subsystem has been determined to be a vital component of the mobile platform through abstract reliability analysis. A failure of a wheel mechanism may prevent the removal of the chassis from the reactor work site, which may be hazardous to potential repairmen. Our goal is to detect as many such faults as possible before they become serious, minimizing the risk to the robot. Our research group is working with Foster-Miller Technologies Incorporated, an organization with considerable experience in evaluating the reliability of hydraulic systems, to develop effective sensor configurations and data analysis procedures for hydraulic wheel actuators and implement them on a testbed system under construction at Foster-Miller. The results of this project can then be used to enhance the reliability of existing and future robots.

The system we are considering consists of a rotary hydraulic motor connected to a 3000 PSI hydraulic power supply through a hydraulic spool valve, as seen in figure 2.1. This system has considerable advantages as an actuator in a nuclear environment. Hydraulic systems are rugged and powerful, and much less likely to produce dangerous sparks than an electrical system. However, hydraulic systems are vulnerable to many faults that electrical systems do not experience, and are much harder to model due to their inherently nonlinear nature.

2.1 Notation

The following variable names are used in this paper:

- A, B, and C are the canonical discrete time state space system matrices
- B_m is the viscous damping coefficient
- $C_{tm} = c_{em} + c_{im}$ represent total, external, and internal leakage, respectively
- d_m is the volumetric displacement of the motor
- J_t is the inertia of the motor and load
- K_f, k_q and k_c are valve flow coefficients
- $M = k_c + C_{tm}$ is a generalized pressure coefficient
- p_l and $p(k)$ are the continuous and discrete pressure drops across the motor
- p_s is the hydraulic power supply nominal pressure of 3000 PSI
- Q is the net fluid flow into the spool valve
- t is the continuous time variable, k the discrete time variable, Δt is the time step
- T_g is the torque generated by the motor
- T_l is the load torque
- *V1* through *V4* are linear AR tests, *NV3* and *NV4* are nonlinear tests, *PLV3* is a piecewise linear AR test
- v_t is the volume of fluid within the motor
- x_v and $x(k)$ are the servovalve position
- $\underline{y}(k)$ is the state vector
- β_e is the bulk modulus of the hydraulic fluid
- θ_m and $\theta(k)$ are the position of the motor shaft
- ρ is the hydraulic fluid density

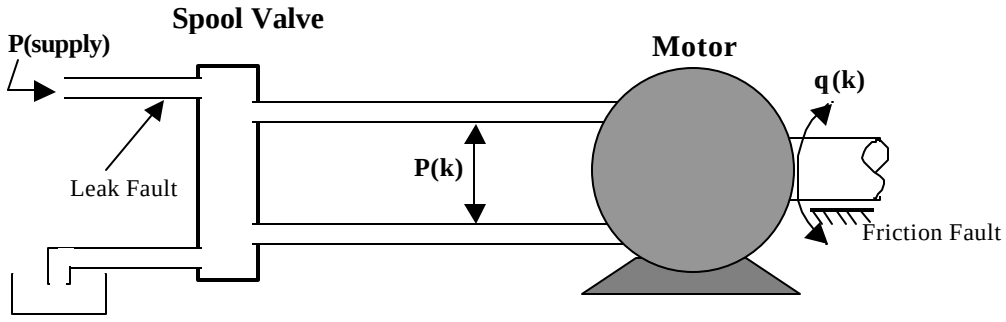

Figure 2.1: Hydraulic System Testbed

The equations for modeling this system are as follows:

$$T_g = p_l d_m = J_t \ddot{\theta}_m + B_m \dot{\theta}_m + T_l ,$$

$$Q = x_v K_f \sqrt{\tfrac{2}{r}(p_s - p_l)} = d_m \dot{q}_m + (c_{im} + c_{em}) p_l + \frac{v_t \dot{p}_l}{4\beta_e}.$$

These equations have been used to create a Simulink [10] model of the system in question. This model follows the above equations with the additional implementation of supply pressure limits, linear and Coulomb friction, control valve dither and system and sensor noise. Several faults have been mathematically modeled and built into the system in such a way as to allow analysis of various methodologies before data from the hardware testbed is available. It was used to provide input to all the tests described in the rest of this paper.

It is obvious that the hydraulic flow equations are highly nonlinear, due to the square root and coupling of variables. The standard linearization of this equation is as follows:

$$Q = k_q x_v - k_c p_l = d_m \dot{q}_m + (c_{im} + c_{em}) p_l + \frac{v_t \dot{p}_l}{4\beta_e}.$$

Note that this is not a strict linearization of the flow equation about zero pressure and valve position. Such an equation would not have a backpressure (k_c) term. However, this term helps reduce the error in the regions in which the system is likely to be controlled. Note that the line of zero error in figure 2.2 below is in the middle of the spool valve's operating range. Linearized equations are suitable for use by standard linear control methods. Tuned error tracking control is usually sufficient to deal with any significant differences between the linear model and the nonlinear system, although these differences can be quite significant, as seen in figure 2.2 below:

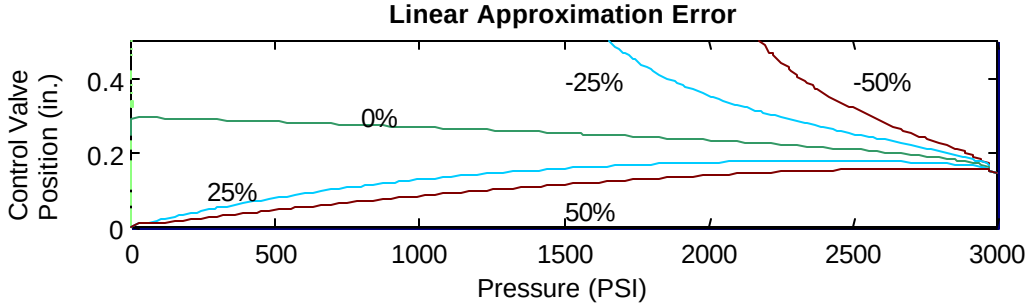

Figure 2.2: Error between original and linearized flow equations

The discrete time state-space control matrices for this system can be obtained as follows:

$$A = \begin{bmatrix} 1 & \Delta t & 0 \\ 0 & \dfrac{J_t - B_m \Delta t}{J_t} & \dfrac{d_m \Delta t}{J_t} \\ 0 & \dfrac{-4\beta_e d_m \Delta t}{v_t} & \dfrac{v_t - 4\beta_e M \Delta t}{v_t} \end{bmatrix}, \quad B = \begin{bmatrix} 0 \\ 0 \\ \dfrac{4\beta_e k_q \Delta t}{v_t} \end{bmatrix}, \quad C = \begin{bmatrix} 1 & 0 & 0 \\ 0 & 0 & 1 \end{bmatrix}.$$

3. Analytical Redundancy

The analytical redundancy (AR) method allows us to explicitly derive the maximum possible number of linearly independent consistency tests for a system [2, 12]. Using a linear model of the system of interest, AR exploits the null space of the observability matrix to allow the creation of a set of test equations. These tests use sensor data histories and known past control inputs to detect any deviation whatsoever from the static or dynamic behaviors of the model. The deviations can then be analyzed for signs that indicate specific faults within the system.

The core of AR is the following equation [2], which is used to determine the systems' observability null space:

$$[\Omega] \begin{bmatrix} Observability \\ Matrix \end{bmatrix} \underline{y}(k) = 0.$$

Ω is the matrix representation of the space which the properly behaving system should never enter. Since most systems will be somewhat noisy and possibly inaccurately modeled, it is likely that the state vector will project slightly into this null space.

For our testbed, using the linearized model equations from the previous section, we can derive the AR tests below:

$$V1 = \frac{B_m \Delta t - J_t}{J_t} \dot{\theta}(k) + \dot{\theta}(k+1) + \frac{-d_m \Delta t}{J_t} p(k) = 0,$$

$$V2 = \left(-1 + \frac{2B_m \Delta t}{J_t} + \frac{-B_m^2 \Delta t^2}{J_t^2} + \frac{4\beta d_m^2 \Delta t^2}{J_t v_t} \right) \dot{\theta}(k) + \left(\frac{d_m B_m \Delta t^2}{J_t^2} + \frac{-2 d_m \Delta t}{J_t} + \frac{4\beta_e d_m M \Delta t^2}{J_t v_t} \right) p(k)$$
$$+ \dot{\theta}(k+2) + \left(\frac{-4\beta d_m k_q \Delta t^2}{J_t v_t} \right) x(k) = 0,$$

$$V3 = \frac{4\beta_e d_m \Delta t}{v_t} \dot{\theta}(k) + \frac{4\beta_e M \Delta t - v_t}{v_t} p(k) + p(k+1) + \frac{-4\beta_e k_q \Delta t}{v_t} x(k) = 0,$$

$$V4 = \left(\frac{-4\beta_e B_m d_m \Delta t^2}{J_t v_t} + \frac{8\beta_e d_m \Delta t}{v_t} + \frac{-16\beta_e^2 d_m M \Delta t^2}{v_t^2} \right) \dot{q}(k) + p(k+2)$$
$$+ \left(-1 + \frac{4\beta_e d_m^2 \Delta t^2}{J_t v_t} + \frac{-16\beta_e^2 M^2 \Delta t^2}{v_t^2} + \frac{8\beta_e M \Delta t}{v_t} \right) p(k)$$
$$+ \left(\frac{-4\beta_e v_t k_q \Delta t + 16\beta_e^2 M k_q \Delta t^2}{v_t^2} \right) x(k) - \left(\frac{4\beta_e k_q \Delta t}{v_t} \right) x(k+1) = 0.$$

These tests correspond to descretized versions of our model equations (*V1* is torque equation, *V3* is flow equation) and their first derivatives (*V2* and *V4*).

Figures 3.1 and 3.2 below show the pressure and velocity responses of the system to both a normal ramp x_v input and the same input with a leak fault that reduces the net flow to half its former value at t = 9s. Note that for these plots and all plots following the non-time variable has been scaled in such a way to give results of small magnitude, thus facilitating plot reading. However, great care has been taken to preserve *relative* scales between plots of the same AR tests, so that they may be compared to each other without bias. (All ***X****V3* tests use the same scale, for example.)

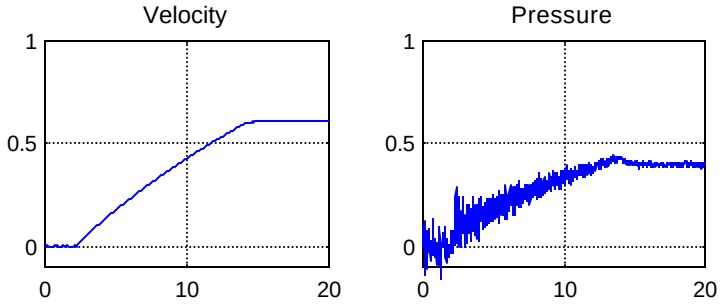

Figure 3.1: Fault Free operation, ramp input.

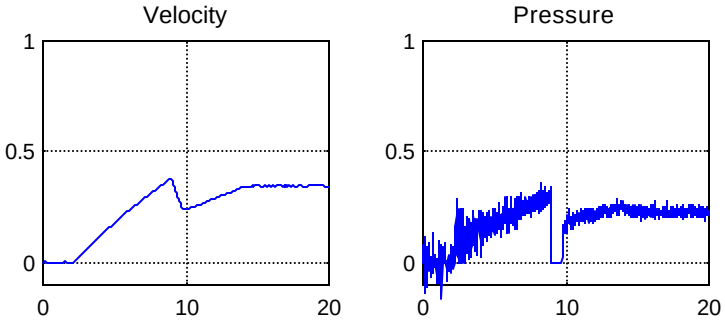

Figure 3.2: Leak Fault at t = 9s, ramp input.

Figure 3.3 shows the results of the *V3* linearized model test in response to the above inputs. (We choose to focus on this test because it is the most straightforward of the linearized tests.) The trend of the test away from its nominal zero-centered value in the

first plot is due to the differences between the linear test and the nonlinear system it is attempting to model. This is undesirable, as it may mask an actual fault that will also cause the V3 linearized AR test to drift in that direction. The second plot shows the effect of a leak fault on the V3 test. Although this is a sudden, serious, fault, note that the magnitude of the change is the same as that of the drift.

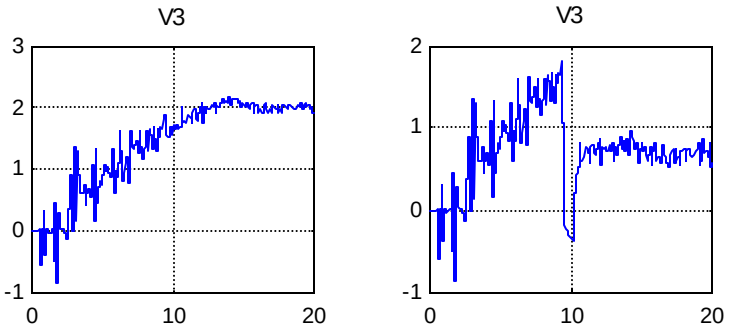

Figure 3.3: Response of AR test V3 to fault free and leak fault ramp inputs seen above. (Figures 3.1 and 3.2)

4. Extension of AR to Nonlinear Systems

Analytical redundancy uses the standard linear state-space control model to derive a set of consistency tests that detect any deviation from this model. This is especially convenient from a control theory point of view since state space control is a well-developed field, allowing one to derive AR tests as a simple addition to the required construction of the system controller. Additionally, it results in AR tests that are substantially similar to the control equations, making it considerably easier to comprehend what the physical significance of the tests is. For example, in the tests above, it was possible to determine the relationship of every test to the model equations.

However, nonlinear model equations are not compatible with the state space method, and thus it is impossible to perform an AR analysis of a nonlinear system using existing methods. The system must be linearized, and as we demonstrate in this paper, this results in AR tests that are inferior to the basic consistency tests derived from simply tracking the compliance of the model with the nonlinear model equations. At the same time, it is not obvious that it is theoretically justifiable to use nonlinear model equations in place of linear model equations that may result from an AR analysis. The analysis is only strictly applicable to the linear system.

One way to attempt to circumvent this is to run several AR tests for the system linearized about different sets of control variables. Each set would be theoretically robust, and in the local region each set would be more accurate than a general linearization of the control equations for the entire workspace. An example of this technique, and the improvement it brings, is illustrated below in figure 4.1. In this case, the pressure-valve position workspace in which the flow equation is nonlinear is divided up into nine equal

regions. The model equation is linearized about a point at the center of each and normal AR tests are derived. (Actually, due to the symmetry of the system, only four linearizations are needed.) During operation, the AR test used is the one that was linearized about a point closest to the current position, with interpolated transitions near the borders of each region.

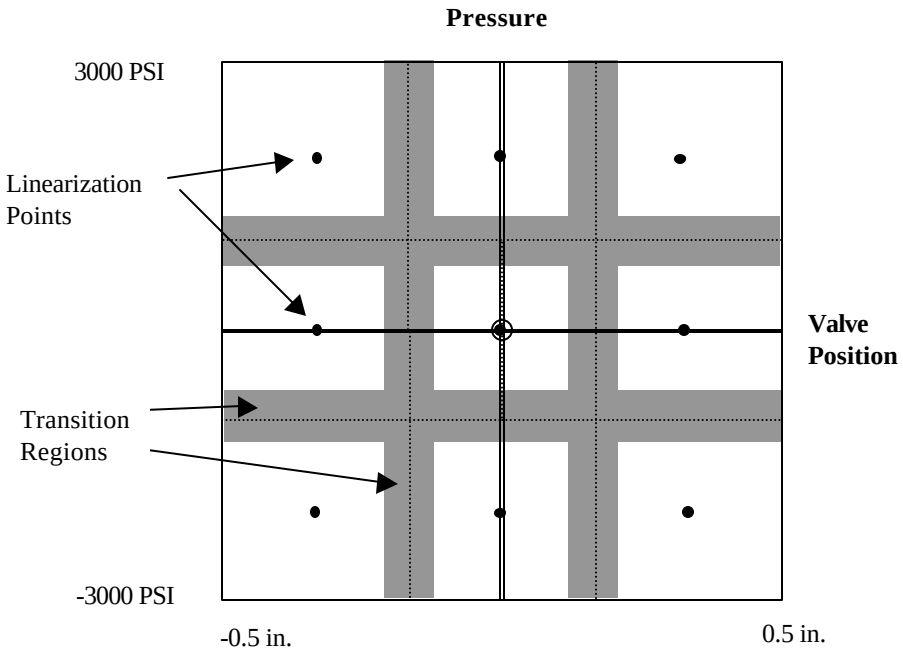

Figure 4.1:Piecewise Linear division of workspace

In response to the same tests as in the previous section, the piecewise linear tests gave the results seen in figure 4.2. The first plot is for normal operation. The second plot is the response of the system to the same fault as the linear AR test in the previous section.

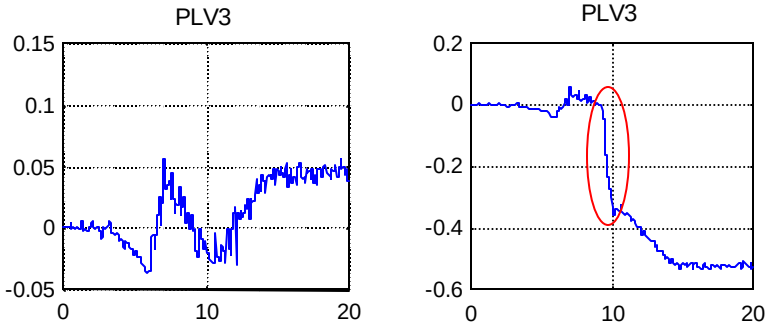

Figure 4.2:Piecewise Linear AR test results for inputs from figure 3.1 and 3.2.

Note that the drifting behavior of the linear test has been drastically reduced from figure 3.3. Before the test can drift far from the point about which it was linearized, the system transitions into another, more appropriate AR test linearized about a point closer to the actual state of the system. This results in a fault signature (circled) that is an order of magnitude larger than the signal produced by the drifting within the regions and the transitions between them, making the fault much easier to detect.

Each partition would use a different linearization of the control equations, but it is important to note that the different linearizations will all share the same basic form, differing only in the values of various constants. This means that the form of the AR tests generated by the different linearizations will also be of the same form. In fact, they will share the relationship to the original model that the globally linearized system possessed! For example, in our system there will always be a test corresponding to the linearized flow equation, only differing in the point about which it is linearized.

Now if we take the partition method to its logical extreme by taking smaller and smaller partitions, the above discussion makes it clear that we will in the limit approach the nonlinear model equations! This means we can in principle justify using the nonlinear model equations in an AR context. Similarly, the AR tests that correspond to derivatives (*V2* and *V4*) of the linear model equations (*V1* and *V3*) can be shown to be more accurately represented by the derivatives of the nonlinear ones. In fact, the nature of the AR method insures that all tests derived from it can be related somehow to the initial system equations, so in theory any tests resulting from a linearized equation can be converted back to a more accurate nonlinear equation.

As linear AR resulted in the model equations and their first derivatives, the nonlinear AR tests are the nonlinear model equations and their first derivatives. Since only the flow equation was nonlinear, we only need two new AR tests, seen below.

$$NV3 = \frac{4\beta_e d_m \Delta t}{v_t}\dot{q}(k) + \frac{4\beta_e C_{tm}\Delta t - v_t}{v_t}p(k) + p(k+1) + \frac{-4\beta_e k_q \Delta t}{v_t\sqrt{p_s}}x(k)\left(\sqrt{(p_s - p(k)}\right) = 0,$$

$$\begin{aligned} NV4 = {} & \left(\frac{4\beta_e d_m \Delta t}{v_t}\right)\left(\dot{q}(k+1) - \dot{q}(k)\right) + p(k+2) + \left(-2 + \frac{4\beta_e C_{tm}\Delta t}{v_t}\right)p(k+1) \\ & + \left(1 - \frac{4\beta_e C_{tm}\Delta t}{v_t}\right)p(k) + \left(\frac{-4\beta_e k_q \Delta t}{v_t\sqrt{p_s}}\right)\left(x(k+1) - x(k)\right)\sqrt{(p_s - p(k))} \\ & + \left(\frac{4\beta_e k_q \Delta t}{v_t\sqrt{p_s}}\right)x(k)\frac{\left(p(k+1) - p(k)\right)}{\sqrt{(p_s - p(k))}} = 0. \end{aligned}$$

In response to the same inputs as the previous two flow equation tests, *NV3* produced the results seen in figure 4.3. Note how large the fault signal (circled) is relative to the noise in the fault-free test run.

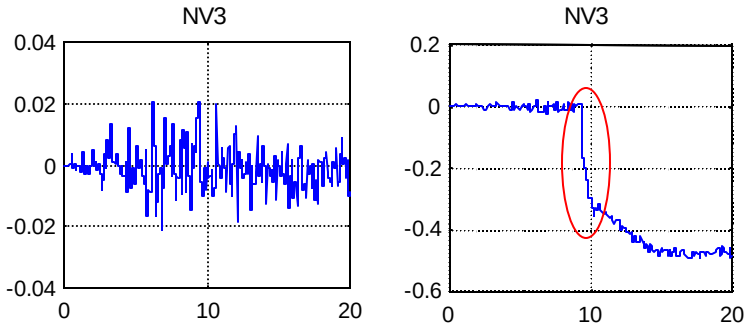

Figure 4.3:Nonlinear AR test results to inputs from figure 3.1 and 3.2.

5. Response of AR Tests to System Faults

Additional simulated results from our nonlinear AR models of the testbed are shown in the Appendix and discussed below. First we see the results of all four AR tests (*V1*, *V2*, *NV3*, and *NV4*) for fault free ramp input in figure A.1. *V1* and *V2* suffer a small drift due to unmodelable friction effects and the flow based AR tests are performing well. The step input in figure A.2, however, shows large spikes in the AR tests even during fault free operation. While unfortunate, this effect is unavoidable for any similarly violent input, since the AR tests are operating on a timeframe much larger than the control input. This test is useful to provide a contrast between the error signals caused by such strong control inputs and actual faults in the system.

Next we look at an example system fault – a fairly serious leak in the hydraulic system, resulting in a drastic loss of power and performance. A quick perusal of the AR test results seen in figures A.3 and A.4 will show that an important characteristic of this kind of failure is a sharp change in every test but *NV4*. A look at the equations shows that *NV4*'s sensitivity to the flow coefficient k_q is dependent on the first derivative of x_v, which changes only slowly in most situations. Note that the magnitude of these signals is smaller than the signal for the step input, so this distinction may prove quite useful.

Next we see the results of a friction fault, representing a jamming or sticking in the wheel mechanism, in figures A.5 and A.6. It is interesting to note that this fault results in negligible signals in most tests except *V1* at the time of occurrence, but causes large signals when the ramp levels off. The tests in question show a strong response when there is a change in acceleration. This suggests that a change in only the first AR test suggests a friction fault. It also gives us a good way to test this suspicion.

The final set of figures, A.7 and A.8, show the response of the AR tests to a 10% increase in the model parameters used by the simulation, without changing the parameters used by

the AR tests. Note the small change in response, indicating the general robustness of the AR method.

Despite the large improvement in AR performance when extended nonlinearly as seen above, we still wish for greater thoroughness in the overall mathematics. Our extension method is ideal for getting the best results out of linear AR applied to a nonlinear system, but does not actually constitute nonlinear AR. The null space that is generated by our state-space methods is a linear null space of a linear system. We can approximate the nonlinear system by taking dense samples and linearizing at many points, eventually taking the nonlinear equations as a limit, but in the process we are still restricting ourselves to the linear dependencies of the system. We would like to know the full shape of the nonlinear system's null space.

6. Conclusions and Future Work

The analytical redundancy technique for fault detection is a promising and theoretically robust method for use in well-modeled linear systems. It provides the theoretical maximum amount of information regarding the deviation of such a system from its expected behavior. The work presented in the above section shows the effectiveness of this method for detecting important system faults.

However, AR is not as useful for dealing with nonlinear systems, since too much information is lost in the linearization of the system so that the state space model can be used. AR only detects how far the system deviates from the model – if the model starts out considerably different due to linearization, there is little information to be gained.

Our method of extending linear AR into the nonlinear domain reduces this problem considerably. We bring the model back in tune with the system, so our tests become much more sensitive and meaningful. With this method, we can create meaningful AR tests for a nonlinear system. However, in the process we lose some of the theoretical robustness inherent in the original linear AR technique. The null space we are interested in is the null space of the nonlinear system, the one we are examining is an extension of the null space of a linearized version of the system. This prevents us from being entirely satisfied with the technique.

An obvious solution to this is to consider a truly nonlinear AR technique, where the null space of the original nonlinear system is considered. This will require considerable use of nonlinear control techniques, and promises to be an exciting avenue for future research. Our other major avenue of interest for the future of this topic is the integration and testing of our techniques on the physical testbed under construction at Foster Miller Technologies. We anticipate that this platform will be useful in refining and expanding these techniques.

Appendix

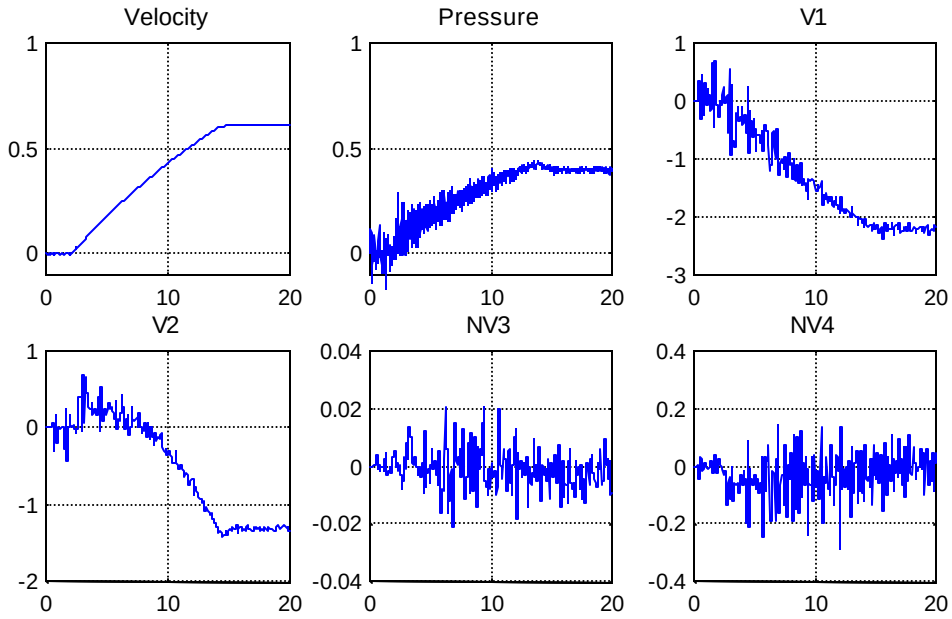

Figure A.1: Fault free ramp input. (Same parameters as figure 3.1.)

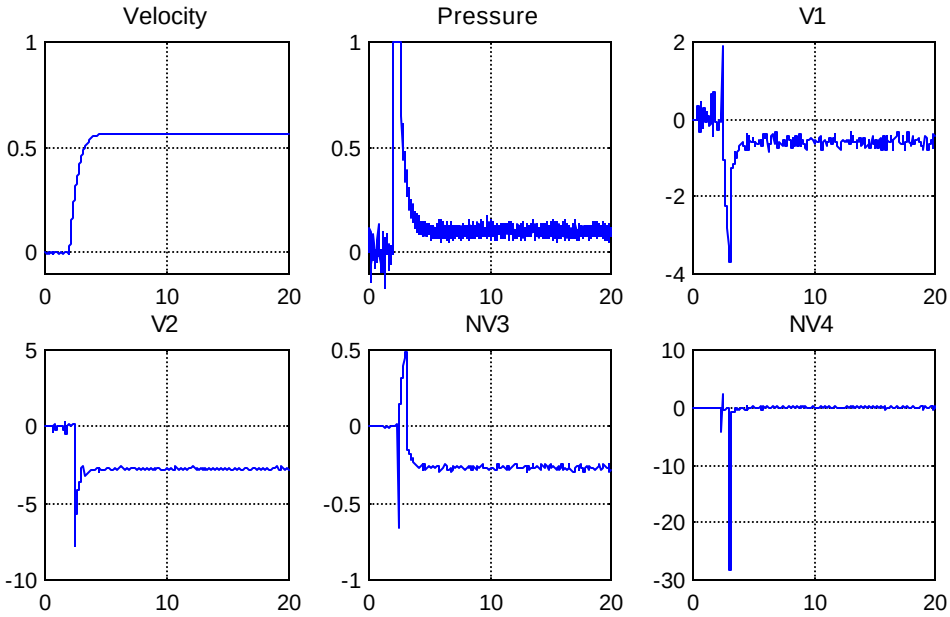

Figure A.2: Fault free step input. Note large AR signals in response to sudden, large changes in input.

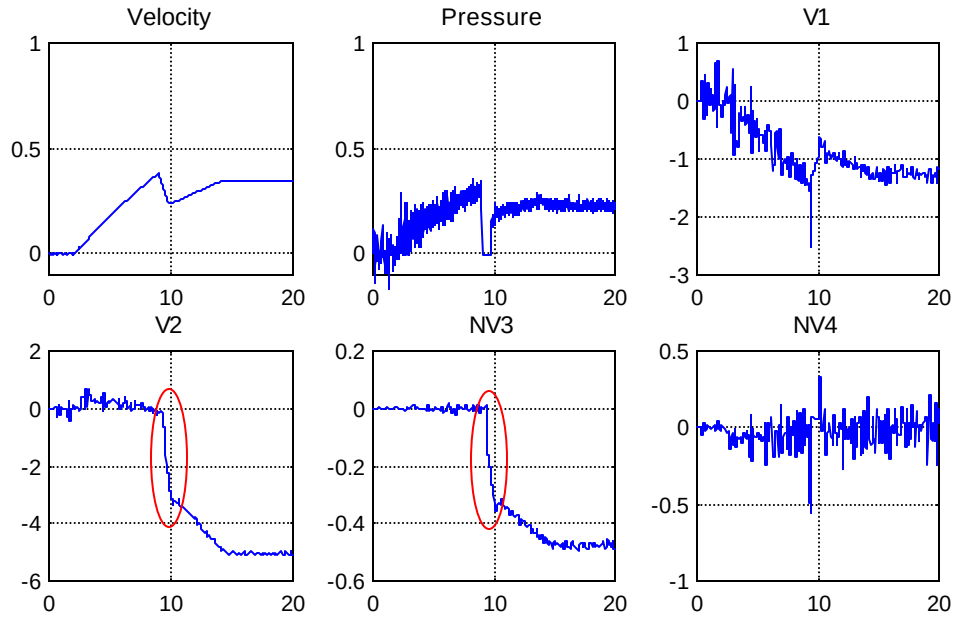

Figure A.3: Leak Fault at t=9, Ramp Input. Note large, clear signals in V2 and NV3.

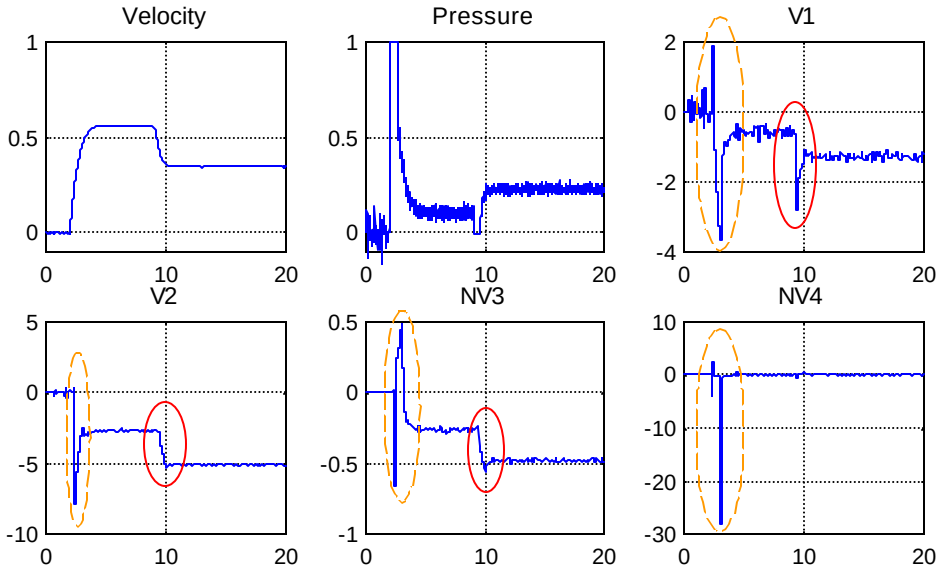

Figure A.4: Leak fault at t=9, step input. Note large AR signals (orange, dashed) at t=2s, when step begins. Fault signal (red) is smaller, but behaves.

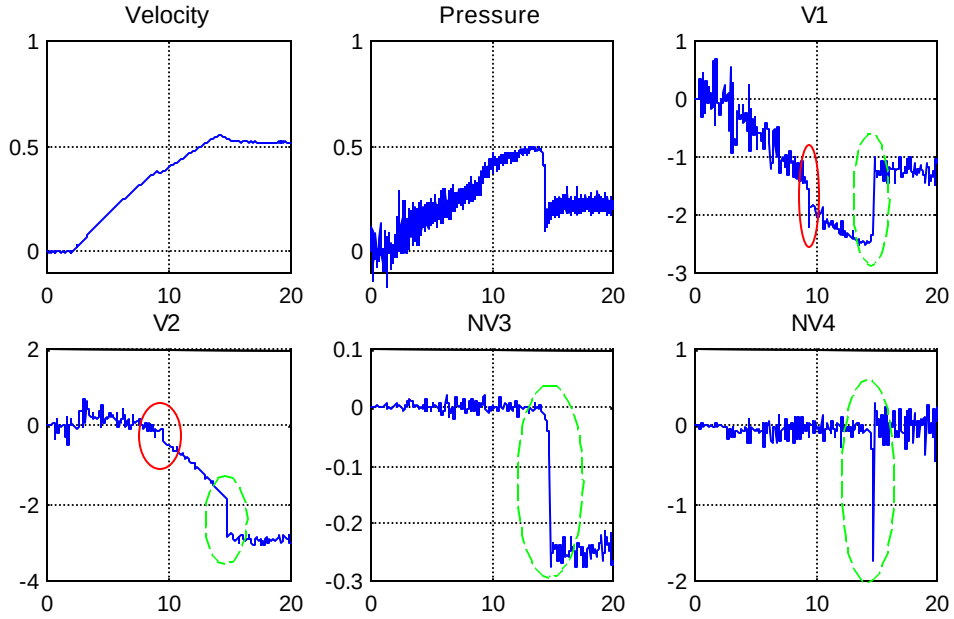

Figure A.5: Friction fault at t=9s, ramp input. Note small initial response (red) and larger response when system stops accelerating (green, dashed).

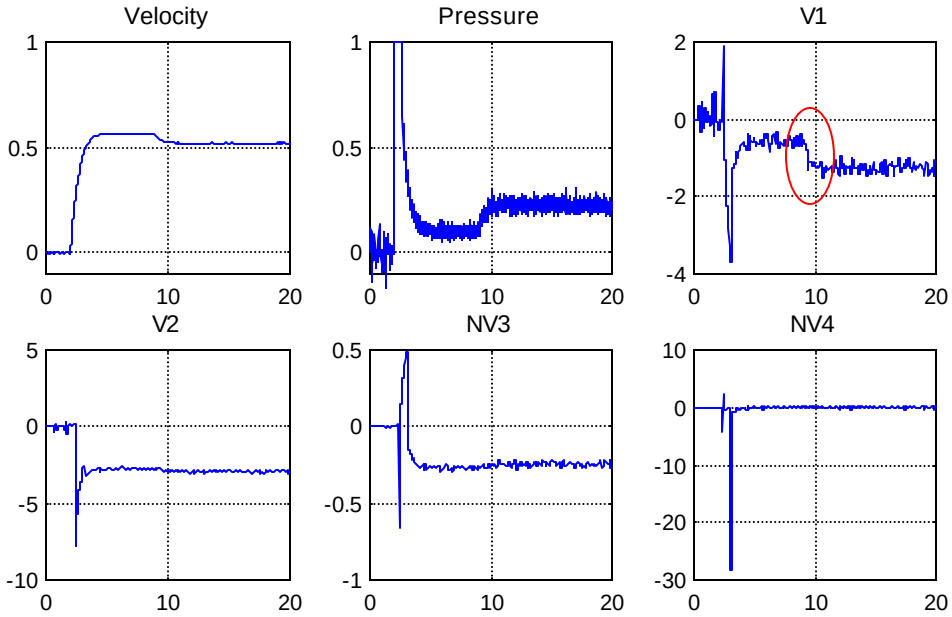

Figure A.6: Friction fault at t=9s, step input. Note virtually no response from any test besides V1 to fault.

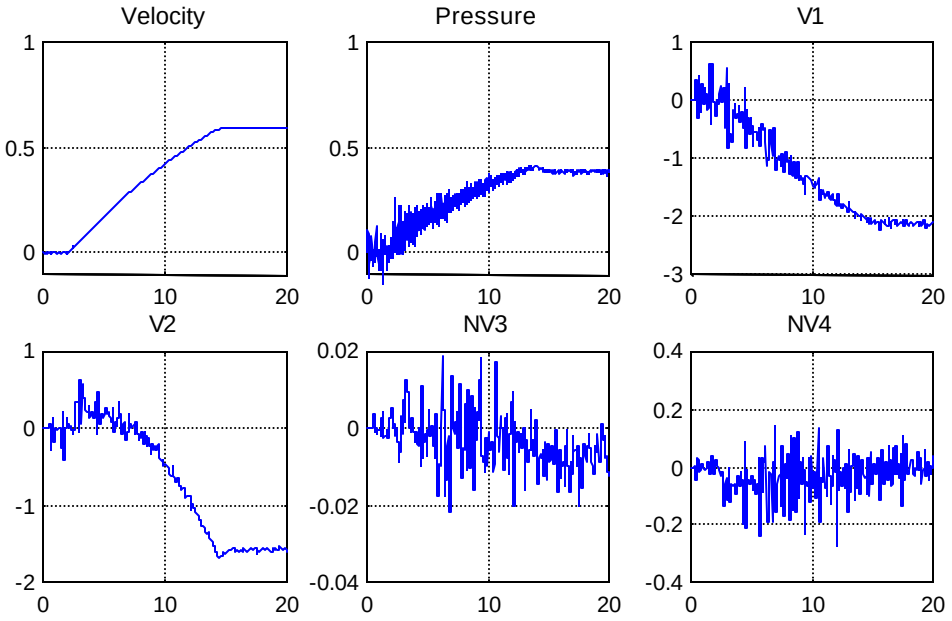

Figure A.7: 10% Parameter estimation error, ramp input. Note strong similarity between this set of signals and figure A.1

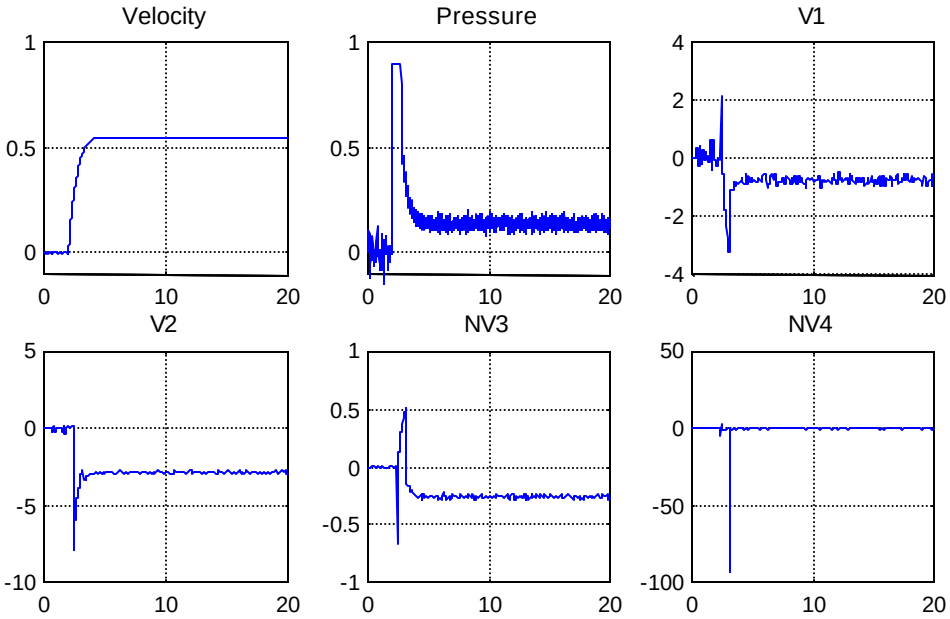

Figure A.8: 10% Parameter estimation error, step input. Compare to figure A.2.

Acknowledgements

This work was supported in part by the National Science Foundation under grants IRI-9526363 and CMS 9796328, by DOE Sandia National Laboratory Contract #AL3017, and DOE contract DE-FG07-97ER 14830.

References

[1] L.C. Bares, L.S. Conley, and B.R. Thompson. Rosie: A Mobile Worksystem for D&D: Overview of System Capabilities and CP-5 Reactor Application. In *Proceedings of the ANS 7th Topical Meeting on Robotics and Remote Systems*, pages 471-477, Augusta, GA, April-May 1997.

[2] E.Y. Chow and A.S. Willsky. Analytical Redundancy and the Design of Robust Failure Detection Systems. *IEEE Transactions on Automatic Control*, AC-29(7):603-614, July, 1984.

[3] L. Conley, W.R. Hamel, and B.R. Thompson. Rosie: A Mobile Worksystem for Decontamination and Dismantlement Operations. In *Proceedings of the ANS 6th Topical Meeting on Robotics and Remote Systems*, pages 231-238, Monterey, CA, February 1995.

[4] Department of Energy, Washington. D.C., *Environmental Restoration and Waste Management 5-Year Plan, Fiscal Years 1994-1998*, January, 1993. DOE/S-00097P, Vol.1-2.

[5] Department of Energy, Federal Energy Technology Center, Morgantown, WV. *Environmental Waste Management Fact Sheet*, October 1997. http://www.fetc.doe.gov/publications/factsheets/ewm/index.html.

[6] B.S. Dhillon. *Robot Reliability and Safety*. Springer-Verlag, New York, NY, 1991.

[7] B.M. Harpel, J.B. Dugan, I.D. Walker, J.R. Cavallaro. Analysis of Robots for Hazardous Environments. In *Proc. IEEE Annual Reliability and Maintainability Symposium*, pages 111-116, Philadelphia, PA, January 1997.

[8] M.L. Leuschen, I.D. Walker, J.R. Cavallaro. Robot Reliability Through Fuzzy Markov Models. In *Proc. IEEE Annual Reliability and Maintainability Symposium*, pages 209-214, Anaheim, CA, January 1998.

[9] M.L. Leuschen, I.D. Walker, J.R. Cavallaro. An Investigation of Reliability of Hydraulic Robots for Hazardous Environments Using Analytical Redundancy. In *Proc. IEEE Annual Reliability and Maintainability Symposium*, Washington, DC, January 1999.

[10] Mathworks. Simulink. http://www.mathworks.com/products/simulink/.

[11] W. Stadler. *Analytical Robotics and Mechatronics*. McGraw-Hill, Inc. New York, NY, 1995.

[12] M.L. Visinsky, J.R. Cavallaro. I.D. Walker. A Dynamic Fault Tolerance Framework for Remote Robots. *IEEE Transactions on Robotics and Automation*, 11(4):477-490, 1995.